Electronic Supplementary Material (ESI) for Dalton Transactions

$Tl(VO)_2O_2(IO_3)_3$: A New Polar Material with A Strong SHG Response

Chao Huang,[a, b] Chun-Li Hu,[a] Xiang Xu,[a] Bing-Ping Yang[a] and Jiang-Gao Mao[a]*

Table S1. Dipole moments for iodate groups and VO_6 octahedra and net dipole moments for the unit cells in $A(VO)_2O_2(IO_3)_3$ (A = K, Rb, Cs, NH4, Tl).

K compound					
Polar unit	Polar unit number in a unit cell	Dipole moment (μ, unit: Debye)			
		x-component	y-component	z-component	Total magnitude
$I(1)O_3$	4	0	±14.70	2.12	14.85
$I(2)O_3$	8	±0.91	±5.92	12.85	14.17
VO_6	8	±1.12	±5.43	2.15	5.95
Net dipole moment in a unit cell		0	0	128．48	128．48
Rb					
Polar unit	Polar unit number in a unit cell	Dipole moment (μ, unit: Debye)			
		x-component	y-component	z-component	Total magnitude
$I(1)O_3$	4	0	±15.73	2.71	15.96
$I(2)O_3$	8	±0.62	±6.08	12.53	13.94
VO_6	8	±0.91	±5.35	2.35	5.92
Net dipole moment in a unit cell		0	0	129.88	129.88
Cs compound					
Polar unit	Polar unit number in a unit cell	Dipole moment (μ, unit: Debye)			
		x-component	y-component	z-component	Total magnitude
$I(1)O_3$	4	0	±15.17	2.96	15.46
$I(2)O_3$	8	±0.19	±6.15	12.03	13.51
VO_6	8	±0.87	±4.83	2.17	5.37
Net dipole moment in a unit cell		0	0	125．44	125．44
Ammonium compound					

Polar unit	Polar unit number in a unit cell	Dipole moment (μ, unit: Debye)			
		x-component	y-component	z-component	Total magnitude
$I(1)O_3$	4	0	±15.83	2.89	16.09
$I(2)O_3$	8	±0.13	±7.21	12.94	14.82
VO_6	8	±1.19	±5.17	2.69	5.94
Net dipole moment in a unit cell		0	0	136．6	136．6
Tl					
Polar unit	Polar unit number in a unit cell	Dipole moment (μ, unit: Debye)			
		x-component	y-component	z-component	Total magnitude
$I(1)O_3$	4	0	±15.04	2.68	15.28
$I(2)O_3$	8	±0.54	±5.66	12.01	13.29
VO_6	8	±0.80	±5.28	2.14	5.76
Net dipole moment in a unit cell		0	0	123．92	123．92

Table S2. The state energies (eV) of the lowest conduction band (L-CB) and the highest valence band (H-VB) of $Tl(VO)_2O_2(IO_3)_3$.

Compound	k-point	H-VB	L-CB
$Tl(VO)_2O_2(IO_3)_3$	*G* (0.000, 0.000, 0.000)	0	1.62757
	Z (0.000, 0.000, 0.500)	-0.23658	1.80888
	T (-0.500, 0.000, 0.500)	-0.3309	1.8294
	Y (-0.500, 0.000, 0.000)	-0.04087	1.82422
	S (-0.500, 0.500, 0.000)	-0.06797	1.80064
	X (0.000, 0.500, 0.000)	-0.07915	1.79996

	U (0.000, 0.500, 0.500)	-0.13489	1.73027
	R (-0.500, 0.500, 0.500)	-0.28756	1.84705

Table S3. The calculated bond orders of $Tl(VO)_2O_2(IO_3)_3$.

$Tl(VO)_2O_2(IO_3)_3$					
Bond	Bond length	Bond order	Bond	Bond length	Bond order
V-O	1.59332	0.92	V-O	1.88980	0.54
V-O	1.85298	0.52	V-O	1.93874	0.38
V-O	1.99272	0.36	V-O	2.20460	0.22
I-O	1.78249	0.47	I-O	1.79418	0.40
I-O	1.84407	0.31	I-O	1.83219	0.26
I-O	1.86899	0.24			

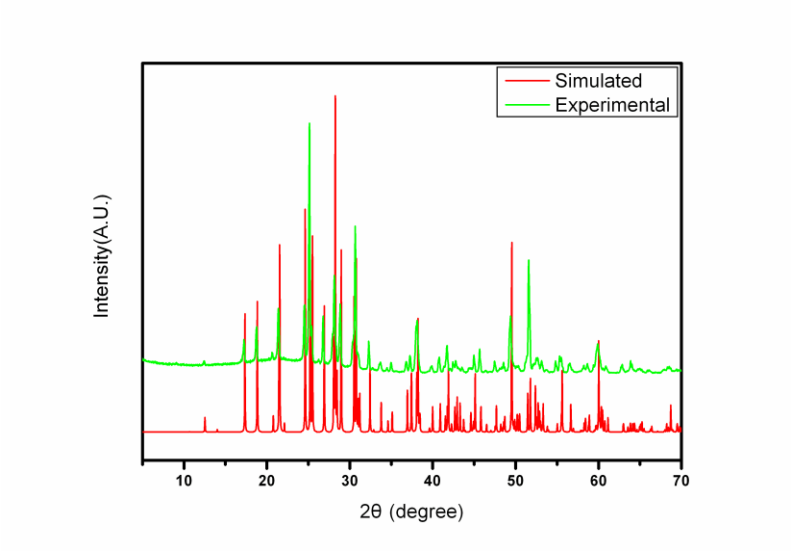

Figure S1. Experimental and simulated powder X-ray diffraction data for $Tl(VO)_2O_2(IO_3)_3$.

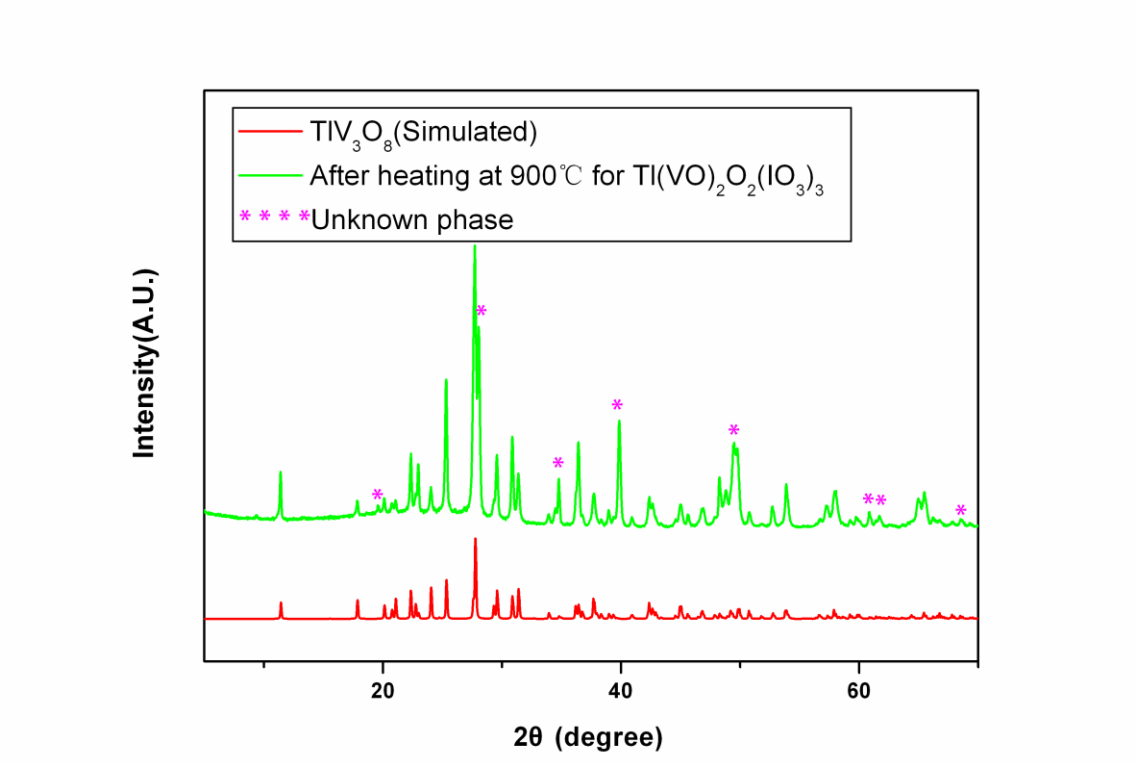

Figure S2. Powder X-ray diffraction studies for the thermal decomposition products of $Tl(VO)_2O_2(IO_3)_3$.

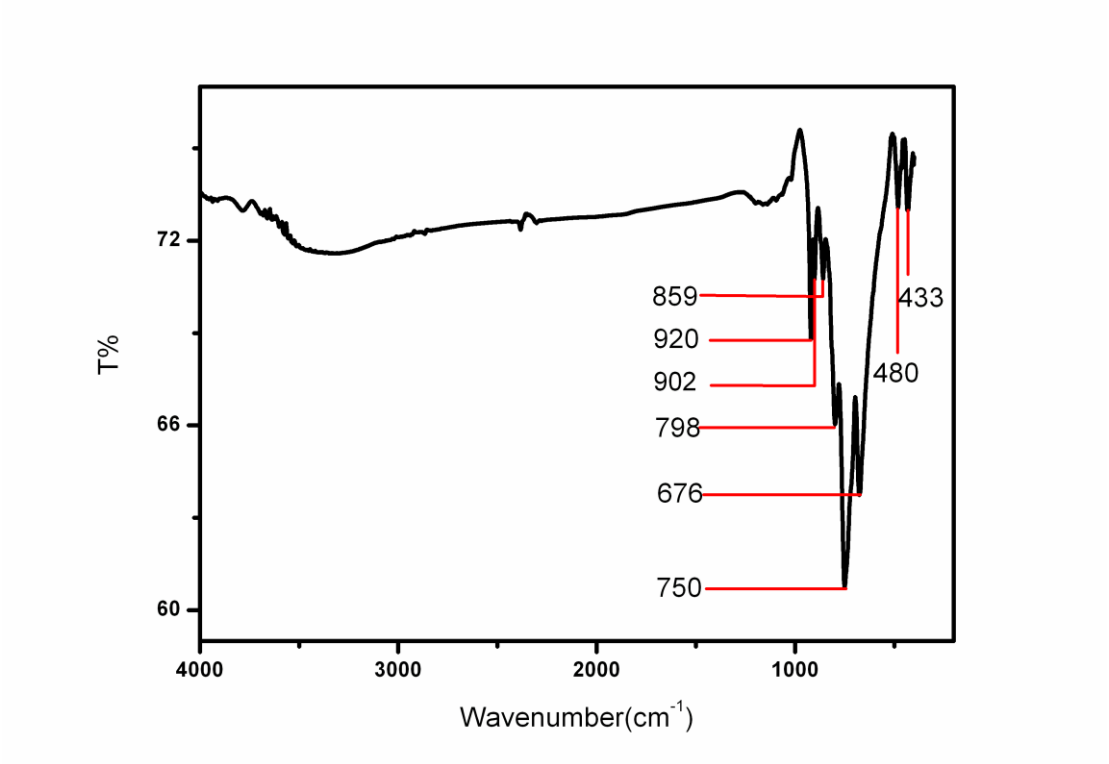

Figure S3. The infrared spectra of $Tl(VO)_2O_2(IO_3)_3$.

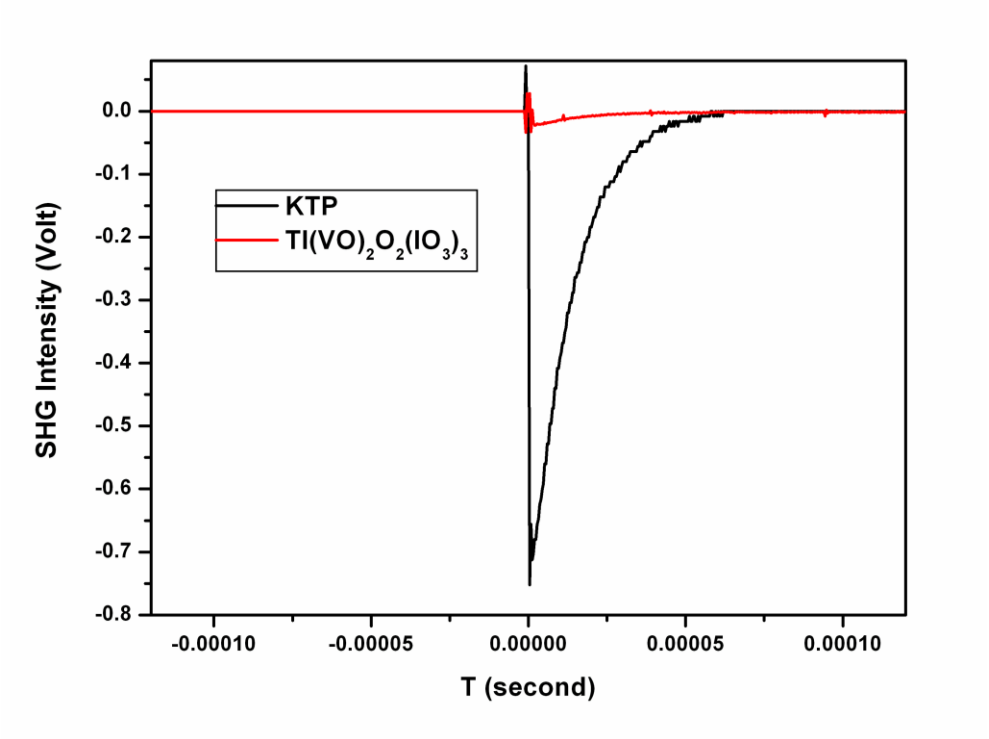

Figure S4. The measured SHG signal of $Tl(VO)_2O_2(IO_3)_3$ in the particle size range of 50-70 mesh compared with that of KTP under 1064 nm laser radiation .

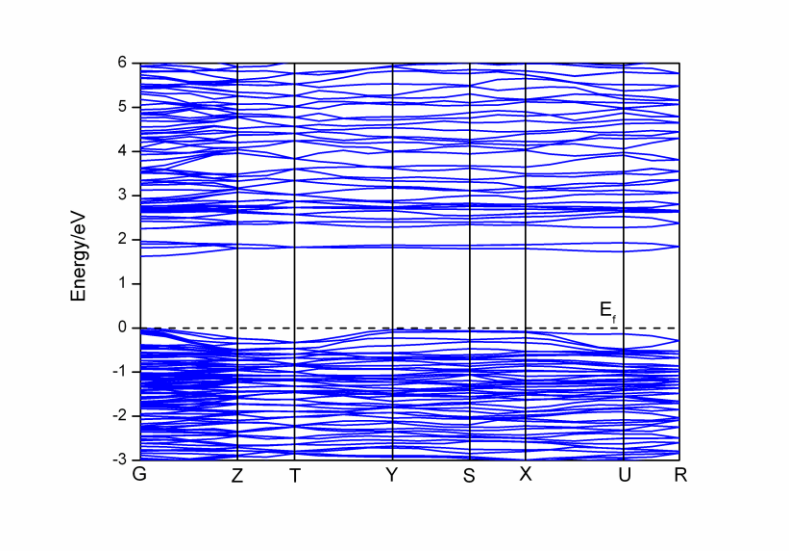

Figure S5. Calculated band structures of $Tl(VO)_2O_2(IO_3)_3$.

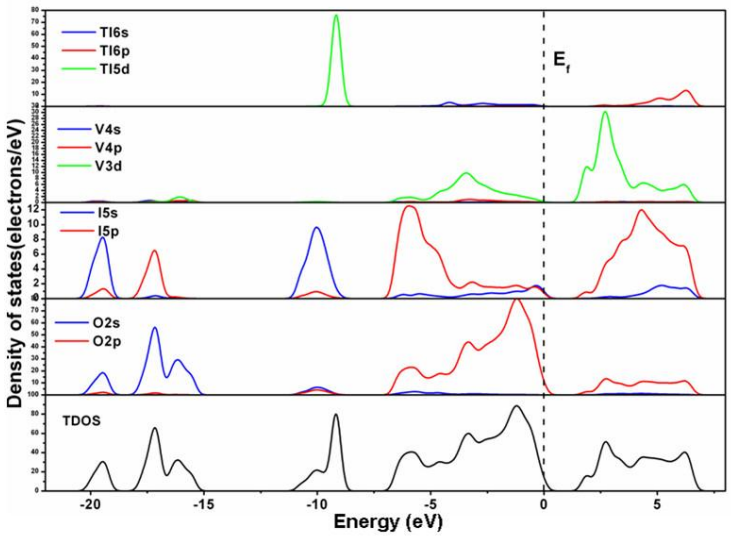

Figure S6. Electronic density of states of $Tl(VO)_2O_2(IO_3)_3$.